3D shot-profile migration in ellipsoidal coordinates

Jeff Shragge and Guojian Shan

ABSTRACT

We present an approach for performing 3D shot-profile migration in ellipsoidal coordinate systems. Wavefields are extrapolated on confocal ellipsoidal shells that are well suited for accurately propagating steeply dipping and turning waves in all azimuthal directions. Numerical implementation of the corresponding dispersion relationship, though, is somewhat problematic due to first-order, complex-valued wavenumbers. We show that an integral transform recasts the problem in a way that eliminates first-order wavenumbers. The corresponding dispersion relationship is similar to that in elliptically anisotropic media. This similarity allows us to use existing implementations of wavefield extrapolation in elliptically anisotropic media to propagate wavefields on ellipsoidal meshes. Impulse response tests demonstrate the stability and accuracy of the approach.

INTRODUCTION

Imaging steeply dipping structure, such as salt flanks, in complex geologic environments remains an issue in 3D seismic migration. Many difficulties arise due to the relate problems of incorrect velocity models and poor downgoing illumination. One strategy is to use turning-wave energy arriving from all azimuths to image the steep dip structure that remains unilluminated by downgoing energy alone. A number of studies have examined this approach with varying degrees of success (**???**).

The practical imaging improvements afforded by imaging turning-wave energy, though, are unavoidably linked to data acquisition geometry and velocity model structure. For example, narrow-azimuth migrations of data sets containing predominantly inline turning-wave energy are usually constrained to have minimal crossline aperture. This restriction precludes imaging turning-wave energy originating from crossline structure arriving at near-zero offsets. The increasing popularity of wide-azimuth acquisition - well suited for recording turning-wave energy from all azimuths - suggests the need for improved wide-aperture wavefield propagation techniques. Determining which seismic imaging methods optimally realize these requirements, both physically and computationally, remains an open research question.

Wave-equation migration (WEM) techniques generally generate superior images relative to other approaches in complex geologic environments. Reverse-time migration, which solves the full acoustic wave equation, is one class of WEM techniques

able to propagate turning waves in all directions (**??**). The computational costs associated with 3D wave propagation and imaging remain significant, though, especially in wide-azimuth contexts. A second class of WEM approaches, based on one-way wavefield extrapolation, rapidly generates solutions to approximate one-way wave equations. The computational advantages of one-way wavefield extrapolation, relative to reverse-time migration, are less obvious when considering the lower accuracy of high-angle propagation and an inherent inability to propagate turning waves by design.

Formulating the seismic imaging problem in more generalized coordinate systems is one way to exploit the computational advantages of one-way wavefield extrapolation while reducing the steep-dip limitations. The general strategy involves extrapolating source and receiver wavefields on meshes oriented toward the wave-propagation direction, generating local images through cross-correlation in the transformed coordinate system, and interpolating the result back to the global image volume. This process is repeated for all source-receiver wavefield pairs. Coordinate transforms proved to be an effective strategy for 2D and 3D plane-wave migration when using tilted Cartesian coordinate systems oriented toward the take-off vector (**??**). **?** apply this strategy in developing a 2D shot-profile migration in confocal elliptic coordinates.

In this paper, we apply the coordinate transform strategy to 3D ellipsoidal meshes. We extrapolate source and receiver wavefields outward in confocal ellipsoidal shells and perform cross-correlations to form local images. In most circumstances the wave-propagation direction is conformal to the ellipsoidal shells, permitting the imaging of turning waves with one-way operators. A second advantage of ellipsoidal coordinate systems is that the inline/crossline aspect ratio is controlled by a single parameter, and meshes can be rescaled to fit either narrow or wide-azimuth geometries. Ellipsoidal coordinates also can be defined using integral transforms that leave the corresponding dispersion relationship no more complicated than that of elliptically anisotropic media. Wavefield extrapolation is thus achieved using numerical approaches similar to optimized elliptically anisotropic finite-difference extrapolation (**?**).

The paper begins with a discussion regarding two definitions of an ellipsoidal coordinate system. We generate the corresponding extrapolation wavenumber appropriate for performing wavefield continuation in ellipsoidal coordinates. We then discuss the implicit 3D finite-difference implementation used to propagate source and receiver wavefields, and give the results of impulse response tests. The paper ends with discussions on future work and the computational overhead associated with performing shot-profile migration in ellipsoidal coordinates.

ELLIPSOIDAL GEOMETRY

A common definition of an ellipsoidal coordinate system denoted by $\boldsymbol{\xi} = [\xi_1, \xi_2, \xi_3]$ relative to a Cartesian mesh given by $\boldsymbol{x} = [x_1, x_2, x_3]$ is (**?**):

$$\begin{aligned} x_1^2 &= \frac{(a^2+\xi_1^2)(a^2+\xi_2^2)(a^2+\xi_3^2)}{(b^2-a^2)(c^2-a^2)}, \\ x_2^2 &= \frac{(b^2+\xi_1^2)(b^2+\xi_2^2)(b^2+\xi_3^2)}{(a^2-b^2)(c^2-b^2)}, \\ x_3^2 &= \frac{(c^2+\xi_1^2)(c^2+\xi_2^2)(c^2+\xi_3^2)}{(a^2-c^2)(b^2-c^2)}. \end{aligned} \tag{1}$$

Parameters a, b, and c are constants defining the coordinate system ellipticity and are constrained by three inequalities: $a^2 < \xi_1^2 < b^2$, $b^2 < \xi_2^2 < c^2$, and $c^2 < \xi_3^2 < \infty$. Surfaces of constant ξ_3 are confocal ellipsoids and represent the direction of wavefield extrapolation, while those of constant ξ_1 and ξ_2 form two- and one-sheeted hyperboloids, respectively. We note that because equations 1 are defined by the squares of the variables, each Cartesian point $\boldsymbol{x}$ is represented by eight ellipsoidal points $\boldsymbol{\xi}$, one located in each octant.

Figures 1 and 2 present two ellipsoidal coordinate examples. In each figure, we infilled the four octants with positive ξ_3 arguments to form a coordinate system appropriate for performing 3D wavefield extrapolation. The difference between the two coordinate systems is controlled by parameter b, where decreasing b leads to a more spherical mesh. Note that in this coordinate system waves can propagate in all azimuthal directions, and usually at low angles to the extrapolation direction in typical Gulf of Mexico velocity profiles.

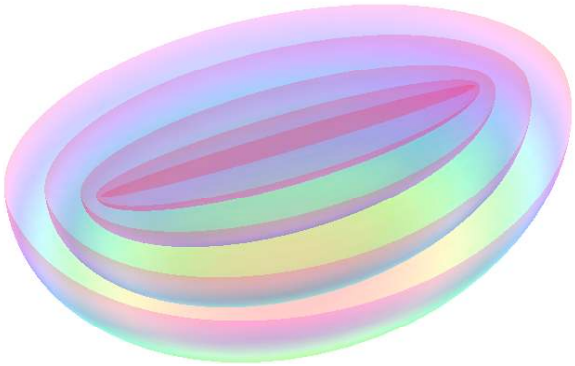

Figure 1: Example of an ellipsoidal coordinate system conforming to narrow-azimuth acquisition geometry created with the parameters $[a, b, c] = [0, 0.995, 1]$. The figure shows five confocal shells. [**NR**]

? define the elliptic-coordinate Helmholtz equation as

$$\begin{aligned} \nabla^2 U = (\xi_3^2 - \xi_2^2) S(\xi_1) \frac{\partial}{\partial \xi_1} \left[S(\xi_1) \frac{\partial}{\partial \xi_1} \right] U + \\ (\xi_1^2 - \xi_3^2) S(\xi_2) \frac{\partial}{\partial \xi_2} \left[S(\xi_2) \frac{\partial}{\partial \xi_2} \right] U + \\ (\xi_1^2 - \xi_2^2) S(\xi_3) \frac{\partial}{\partial \xi_3} \left[S(\xi_3) \frac{\partial}{\partial \xi_3} \right] U = -\omega^2 s^2 U, \end{aligned} \tag{2}$$

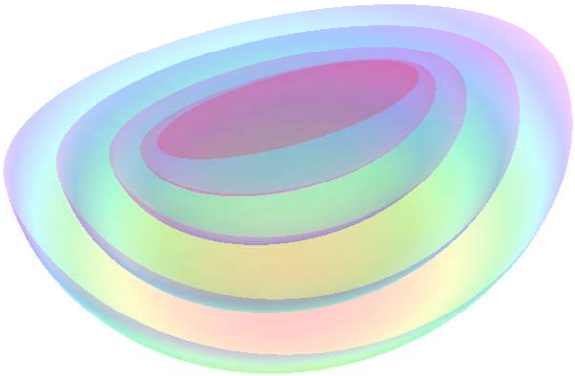

Figure 2: Example of an ellipsoidal coordinate system conforming to wide-azimuth acquisition geometry created with the parameters $[a, b, c] = [0, 0.925, 1]$. The figure shows five confocal shells.[**NR**]

where U is a wavefield, ∇^2 is the Laplacian operator, ω is angular frequency, s is slowness (reciprocal of velocity), and $S(\sigma)$ is a general parameter defined by

$$S(\sigma) = \sqrt{(\sigma^2 + a^2)(\sigma^2 + b^2)(\sigma^2 + c^2)}. \tag{3}$$

Equation 2 contains partial derivatives with respect to the parameter S. This leads to a dispersion relationship of the type studied in **?**,

$$k_{\xi_3} = \mathrm{i}a_3 \pm \sqrt{a_4^2\omega^2 s^2 - a_5^2 k_{\xi_1}^2 - a_6^2 k_{\xi_2}^2 + \mathrm{i}a_8 k_{\xi_1} + \mathrm{i}a_9 k_{\xi_2} - a_{10}^2}, \tag{4}$$

where a_i are geometric coefficients, $\mathrm{i} = \sqrt{-1}$ and k_{ξ_j} is the wavenumber in the corresponding j^{th} axis.

Overall, the ellipsoidal coordinate system as defined in equation 1 is well suited to 3D shot-profile migration in a geometric sense; however, two issues make it difficult to implement accurately. First, the dispersion relationship in equation 4 does not easily lend itself to implicit finite-difference methods because of the imaginary first-order terms (e.g., $\mathrm{i}a_8 k_{\xi_1}$). Second, the octant-based definition introduces non-uniqueness to the coordinate system variables. Overall, making an ellipsoidal coordinate system practical for wavefield extrapolation will require an alternate definition that overcomes these two issues.

Integral Confocal Ellipsoidal Equations

A second definition for confocal ellipsoidal coordinates uses auxiliary variables defined through integral transforms. **?** defines the following Jacobi elliptic integral transforms for each coordinate system axis:

$$\begin{aligned} \beta &= \int_b^{\xi_1} \frac{c\,\mathrm{d}\xi_1}{(c^2-\xi_1^2)(\xi^2-c^2)}, \\ \gamma &= \int_0^{\xi_2} \frac{c\,\mathrm{d}\xi_2}{(b^2-\xi_2^2)(c^2-\xi^2)}, \\ \alpha &= \int_c^{\xi_3} \frac{c\,\mathrm{d}\xi_3}{(\xi_2^2-b^2)(\xi^2-c^2)}, \end{aligned} \tag{5}$$

where axes $[\beta, \gamma, \alpha]$ are conformal to the $[\xi_1, \xi_2, \xi_3]$ axes, but are stretched by the integral transforms defined in equation 5. Axes $[\beta, \gamma, \alpha]$ are defined on the following ranges: $0 \leq \xi_1 \leq \infty$, $0 \leq \xi_2 \leq \infty$ and $0 \leq \xi_3 \leq \infty$. Additional information on the integral transforms can be found in Appendix A. Figure 3 illustrates the relative stretching for each axis for the wide-azimuth geometry case presented in figure 2.

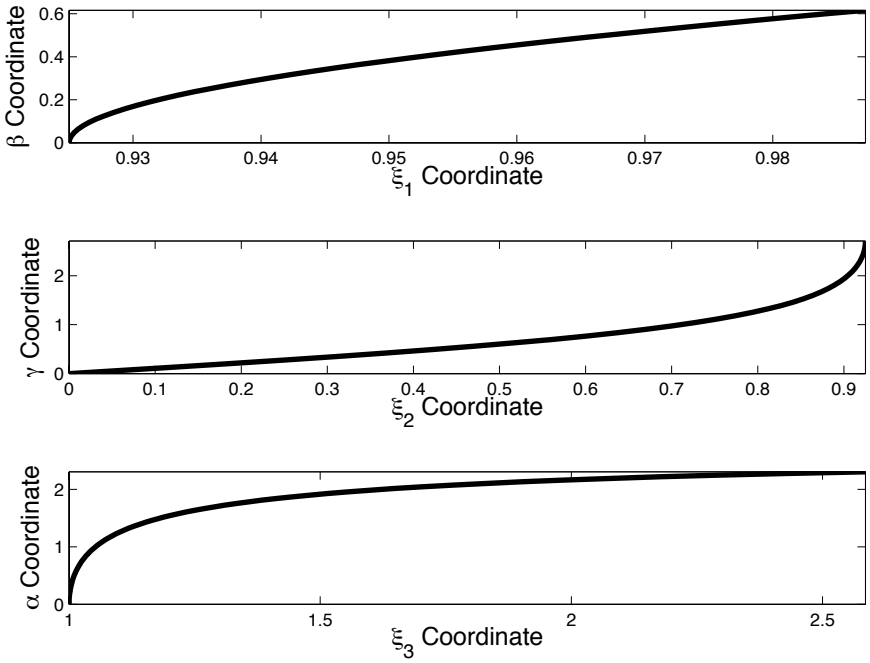

Figure 3: Integral transform stretches for the $\boldsymbol{\xi}$ axes given by equation 5. Top panel: $\beta - \xi_1$ coordinate stretch. Middle panel: $\gamma - \xi_2$ coordinate stretch. Bottom panel: $\alpha - \xi_3$ coordinate stretch.[**NR**]

The integral ellipsoidal-coordinate Helmholtz equation is (**?**):

$$\nabla^2 U = (\xi_2^2 - \xi_3^2)\frac{\partial^2}{\partial \beta^2}U + (\xi_1^2 - \xi_3^2)\frac{\partial^2}{\partial \gamma^2}U + (\xi_1^2 - \xi_2^2)\frac{\partial^2}{\partial \alpha^2}U = -\omega^2 s^2 U. \tag{6}$$

Note that this definition effectively rescales the $\boldsymbol{\xi}$ coordinate axes to eliminate the first-order partial-differential terms in equation 2. This represents the most important theoretical result in this paper, as it removes the main implementation difficulty. In addition, integral ellipsoidal coordinates are defined globally, not just in octants, which eliminates the non-uniqueness noted above.

Obtaining a dispersion relationship from the expression in equation 6 is fairly straightforward. Replacing the partial differential terms with their Fourier-domain counterparts (i.e. $\frac{\partial}{\partial j} \leftrightarrow -\mathrm{i}k_j$, for $j = \alpha, \beta, \gamma$) and solving for the extrapolation direction wavenumber k_α yields

$$k_\alpha = \sqrt{A^2\omega^2 s^2 - B^2 k_\beta^2 - C^2 k_\gamma^2}, \tag{7}$$

where

$$A = \frac{1}{\sqrt{\xi_1^2 - \xi_2^2}}, \quad B = \sqrt{\frac{\xi_2^2 - \xi_3^2}{\xi_1^2 - \xi_2^2}}, \quad \text{and} \quad C = \sqrt{\frac{\xi_1^2 - \xi_3^2}{\xi_1^2 - \xi_2^2}}. \tag{8}$$

In general, equation 7 is inexact because the A, B and C coefficients in equations 8 (and possibly slowness) vary spatially along the β and γ axes.

Relationship to elliptically anisotropic media

A naturally arising concern is whether the dispersion relationship in equation 7 can be implemented accurately and efficiently in a wavefield extrapolation scheme. We address this question by comparing the ellipsoidal and the (Cartesian-coordinate) elliptically anisotropic media dispersion relationships. By defining an effective slowness $s_A = As$ and rewriting equation 7 as

$$\frac{k_\alpha}{\omega s_A} = \sqrt{1 - B^2 \frac{k_\beta^2}{\omega^2 s_A^2} - C^2 \frac{k_\gamma^2}{\omega^2 s_A^2}}, \tag{9}$$

we observe that the ellipsoidal coordinate dispersion relationship resembles that for elliptically anisotropic media (**?**). Specifically, ellipsoidal coordinates relate to the case where Thomsen parameters (**?**) obey $\epsilon = \delta$

$$\left.\frac{k_{x_3}}{\omega s}\right|_{\epsilon=\delta} = \left.\sqrt{\frac{1 - (1+2\epsilon)\frac{k_{x_1}^2 + k_{x_2}^2}{\omega^2 s^2}}{1 - 2(\epsilon - \delta)\frac{k_{x_1}^2 + k_{x_2}^2}{\omega^2 s^2}}}\right|_{\epsilon=\delta} = \sqrt{1 - (1+2\epsilon)\frac{k_{x_1}^2}{\omega^2 s^2} - (1+2\epsilon)\frac{k_{x_2}^2}{\omega^2 s^2}}. \tag{10}$$

From equation 10 we see that equation 7 is no more complex than the dispersion relationship for propagating waves in elliptically anisotropic media, which is now routinely handled with optimized finite-difference approaches (**???**).

3D IMPLICIT FINITE-DIFFERENCE PROPAGATION

A general approach to 3D implicit finite-difference propagation is to approximate the square-root by a series of rational functions (**?**)

$$S_\alpha = \sqrt{1 - B^2 S_\beta^2 - C^2 S_\gamma^2} \approx \sum_{i=1}^{n} \frac{a_i S_r^2}{1 - b_i S_r^2}, \tag{11}$$

where $S_i = \frac{k_i}{\omega s_A}$ for $i = \alpha, \beta, \gamma$, term $S_r^2 = B^2 S_\beta^2 + C^2 S_\gamma^2$, and n is the order of the coefficient expansion. At this point, we do not address the anisotropy generated by the B and C coefficients, as they can be implemented through additional slowness model stretches.

Coeff. order i	Coeff. a_i	Coeff. b_i
1	0.040315157	0.873981642
2	0.457289566	0.222691983

Table 1: Coefficients used in 3D implicit finite-difference wavefield extrapolation.

One procedure for finding an optimal set of coefficients is to solve the following optimization problem (**?**),:

$$\min \int_0^{\sin\phi} \left[\sqrt{1 - S_r^2} - \sum_{i=1}^{n} \frac{a_i S_r^2}{1 - b_i S_r^2} \right]^2 \mathrm{d}S_r, \tag{12}$$

where ϕ is the maximum optimization angle. We generated the following results using a 4th-order approximation and coefficients found in Table 1 (Lee and Suh, 1985).

Extrapolation Algorithm

Using the 4th-order approximation is equivalent to solving a cascade of partial differential equations (**?**)

$$\begin{aligned}
\frac{\partial}{\partial\alpha}U &= \mathrm{i}\omega s U, \\
\frac{\partial}{\partial\alpha}U &= \mathrm{i}\omega s \left[\frac{\frac{a_1 B^2}{\omega^2 s_A^2}\frac{\partial^2}{\partial\beta^2}}{1+\frac{b_1 B^2}{\omega^2 s_A^2}\frac{\partial^2}{\partial\beta^2}} + \frac{\frac{a_1 C^2}{\omega^2 s_A^2}\frac{\partial^2}{\partial\gamma^2}}{1+\frac{b_1 C^2}{\omega^2 s_A^2}\frac{\partial^2}{\partial\gamma^2}} \right] U, \\
\frac{\partial}{\partial\alpha}U &= \mathrm{i}\omega s \left[\frac{\frac{a_2 B^2}{\omega^2 s_A^2}\frac{\partial^2}{\partial\beta^2}}{1+\frac{b_2 B^2}{\omega^2 s_A^2}\frac{\partial^2}{\partial\beta^2}} + \frac{\frac{a_2 C^2}{\omega^2 s_A^2}\frac{\partial^2}{\partial\gamma^2}}{1+\frac{b_2 C^2}{\omega^2 s_A^2}\frac{\partial^2}{\partial\gamma^2}} \right] U.
\end{aligned} \tag{13}$$

We solve these equations implicitly at each $\Delta\alpha$ extrapolation step by a finite-difference splitting method that alternately advances the wavefield in the β and γ directions. Splitting methods allow us to apply the B and C scaling factors directly by introducing rescaled effective slowness models: $s^B_{eff} = \frac{s_A}{B} = \frac{A}{B}s$ and $s^C_{eff} = \frac{s_A}{C} = \frac{A}{C}s$.

One drawback to splitting methods is that they generate numerical anisotropy. To minimize these effects, we apply a Fourier-domain phase-correction filter (**?**)

$$U = U\mathrm{e}^{\mathrm{i}\Delta\alpha k_L}, \tag{14}$$

where

$$k_L = \sqrt{1 - \frac{k_\beta^2}{(\omega s_B^r)^2} - \frac{k_\gamma^2}{(\omega s_C^r)^2}} - \left[1 - \sum_{i=1}^{2} \left(\frac{a_i (\frac{k_\beta}{\omega s_A^r})^2}{1 - b_i (\frac{k_\beta}{\omega s_A^r})^2} - \frac{a_i (\frac{k_\gamma}{\omega s_A^r})^2}{1 - b_i (\frac{k_\gamma}{\omega s_A^r})^2} \right) \right], \tag{15}$$

and s_B^r and s_C^r are reference slownesses chosen to be the mean value of s^B_{eff} and s^C_{eff} defined above.

Impulse Response Tests

We conducted impulse response tests on a 500 x 400 x 400 mesh in a homogeneous medium with slowness $s = 0.0005$ s/m. The initial wavefield consisted of three smoothed point sources at $t = [0.5, 0.75, 1]$ seconds. Using this experimental setup, we expect the impulse responses to consist of three hemispherical surfaces of radii $r = [1000, 1500, 2000]$ meters. We used the narrow-azimuth coordinate system pictured in figure 1.

Figure 4's upper and lower panels show the inline and crossline responses, respectively. To illustrate the accuracy of the approach, we overlaid three lines showing the analytical results. Note that the impulse responses are limited at high angles both by the coordinate system boundaries and by the 50 sample cosine-taper function applied at the edges. Figure 5 shows the 1300 m depth slice. The symmetric response indicates that the Li filter has accounted for the numerical anisotropy from the numerical splitting.

FUTURE WORK

Our main motivation for exploring alternative 3D imaging geometries is to facilitate the propagation of overturning events in all directions. While this study suggests this goal is achievable, we recognize that imaging overturning events is likely to be of greater significance in situations where: i) the illumination from downgoing waves is minimal (i.e. salt body shadow zones); and ii) the seismic data acquisition enables the recording of these events (i.e. wide apertures and long recording times). Currently, SEP has neither a demonstrative wide-azimuth data set (with an isotropic velocity model) for testing purposes nor the computational power to do so. However, the ellipsoidal coordinate shot-profile algorithm will, hopefully, be tested on an appropriate data set using an industrial-sized cluster.

Another issue warranting mention is the additional computational overhead associated with ellipsoidal coordinate shot-profile migration. Below is a short list discussing 3D migration issues in ellipsoidal (ECC) and Cartesian (CCC) coordinate systems:

- Both the inline and crossline migration aperture could be reduced in an ECC because, unlike in a CCC, an ECC spreads out naturally and increases the effective aperture. (Sufficient volume sampling is still required to obtain a good image.)
- Imaging in non-Cartesian coordinate systems require two additional full-volume interpolations, one each between the corresponding velocity models and image spaces. While the former interpolation is easily parallelized, the later requires spraying each ECC image point to a neighborhood of CCC points. This remains difficult to parallelize efficiently, except by expanding the image volume by a factor equal to the number of threads used for interpolation.

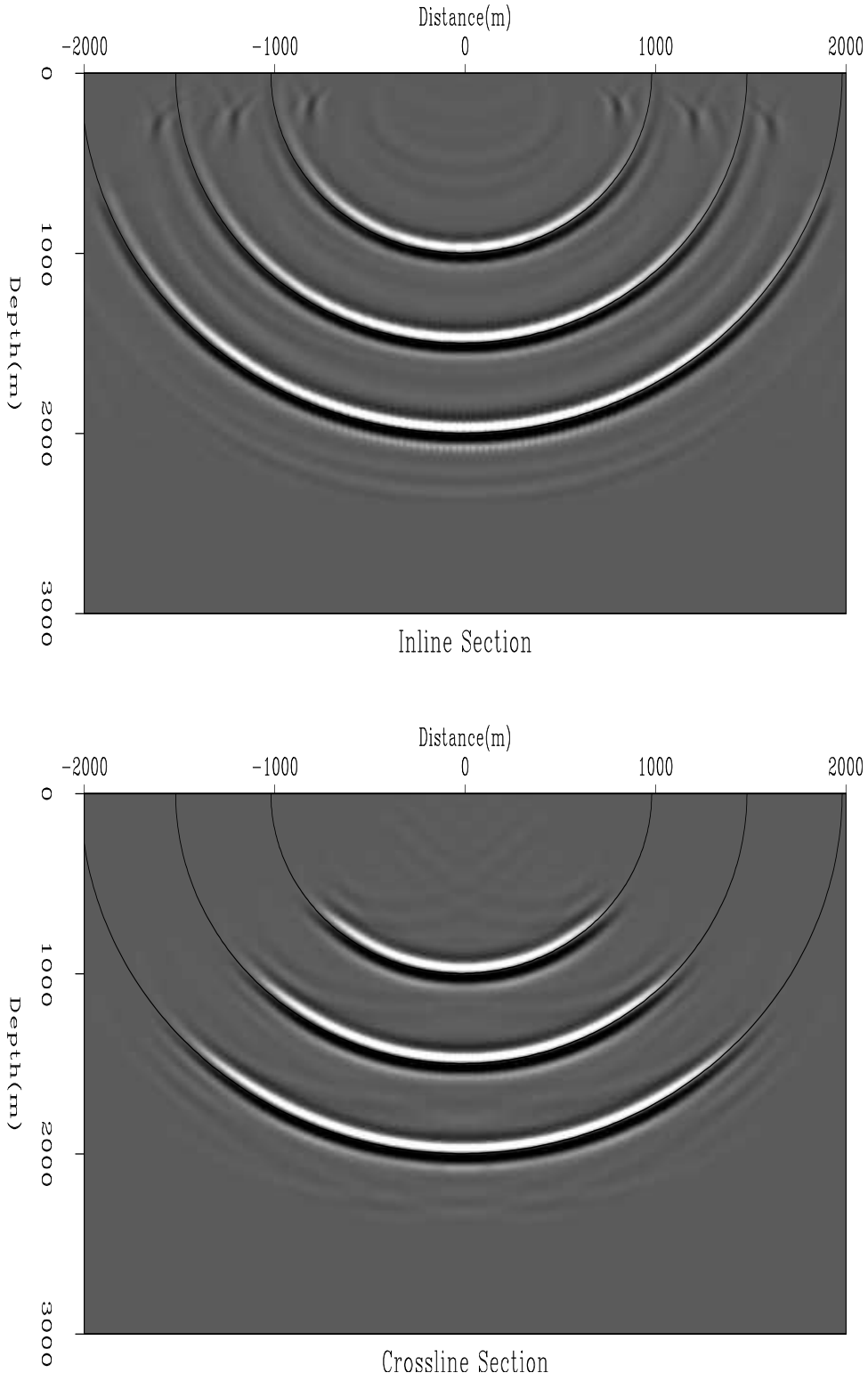

Figure 4: Ellipsoidal coordinate impulse response cross sections through the 3D image volume for the narrow-azimuth ellipsoidal coordinate system defined in figure 1. Top panel: Inline response. Bottom panel: Crossline response. [**CR**]

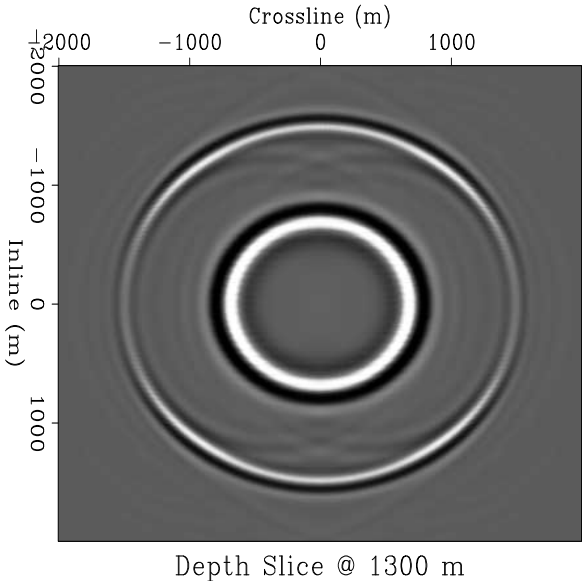

Figure 5: Image volume depth slice taken at 1300m. Note the circular symmetry of the impulse response and the stronger inline amplitudes relative to the crossline. [**CR**]

- Migration costs can be lowered, perhaps by an order of magnitude, by imaging neighboring shot profiles in the same ECC system.
- Because the ECC and CCC originate on the same initial surficial plane, no wavefield injection is required. However, the sampling of the two initial surfaces is different and requires an initial interpolation.

CONCLUSIONS

This paper presents a 3D shot-profile migration approach in ellipsoidal coordinates. The common form of ellipsoidal coordinates generates confocal ellipsoidal shells well-positioned for propagating turning waves in all azimuths. The numerical aspects of implementing the corresponding dispersion relationship, though, are somewhat problematic. We use an integral transform to recast the problem in a way that facilitates numerical implementation. We note that the similarity between the new ellipsoidal and elliptically anisotropic media dispersion relationships allows us to use existing implicit finite-difference extrapolation implementations. The impulse responses demonstrate that the numerical solution is both accurate and stable. Future work will focus on generating 3D shot-profile migration results in the ellipsoidal coordinate system.

ACKNOWLEDGMENTS

We would like to thank Ben Witten for helpful conversations.

REFERENCES

Lee, M. W. and S. Y. Suh, 1985, Optimization of one-way wave-equations (short note): Geophysics, **50**, 1634–1637.

APPENDIX A

INTEGRAL ELLIPTIC REPRESENTATIONS

The integral elliptic representations of the ellipsoidal coordinate system are given by the following three equations (**?**):

$$\begin{aligned}
\beta = \; & c\int_b^{\xi_1} \tfrac{\mathrm{d}\xi_1}{(c^2-\xi_1^2)(\xi_1^2-c^2)} = \; F\left[\sqrt{1-\frac{b^2}{c^2}}, \sin^{-1}\left(\sqrt{\frac{1-\frac{b^2}{\xi_1^2}}{1-\frac{b^2}{c^2}}}\right)\right], \\
\gamma = \; & c\int_0^{\xi_1} \tfrac{\mathrm{d}\xi_1}{(b^2-\xi_1^2)(c^2-\xi_1^2)} = \; F\left[\frac{b}{c}, \sin^{-1}\left(\frac{\xi_2}{b}\right)\right], \\
\alpha = \; & c\int_c^{\xi_2} \tfrac{\mathrm{d}\xi_2}{(\xi_2^2-b^2)(\xi_2^2-c^2)} = \; F\left[\frac{b}{c}, \frac{\pi}{2}\right] - F\left[\frac{b}{c}, \sin^{-1}\left(\frac{c}{\xi_3}\right)\right],
\end{aligned} \tag{A-1}$$

where $F[\cdot]$ are elliptic integrals of the first kind defined by

$$u = F[\phi, k] = \int_0^{\phi} \frac{\mathrm{d}\theta}{\sqrt{1-k^2\sin^2\theta}}, \tag{A-2}$$

where the elliptic modulus k satisfies $0 < k^2 < 1$ and ϕ is the Jacobi amplitude. Solutions to equation A-2 are calculated using the method of arithmetic-geometric mean and descending Landen Transformation described in **?**.

The integral transforms are invertible and can be represented in terms of Jacobi elliptic functions $\mathrm{dc}(u,k), \mathrm{nd}(u,k)$ and $\mathrm{sn}(u,k)$ (**?**):

$$\begin{aligned}
\xi_1 &= b\,\mathrm{nd}\left[\beta, \sqrt{1-\frac{b^2}{c^2}}\right], \\
\xi_2 &= b\,\mathrm{sn}\left[\gamma, \frac{b}{c}\right], \\
\xi_3 &= c\,\mathrm{dc}\left[\alpha, \frac{b}{c}\right],
\end{aligned} \tag{A-3}$$

where k is again elliptic modulus and u is defined by equation A-2. The Jacobi elliptic functions are calculated using the method of the arithmetic-geometric mean described in **?**.